

## Lecture 14: Creep-Resistant Steel, Case Study

### Introduction

Typical operating parameters for steels used in the manufacture of power plant are compared against corresponding values for nickel alloys in aero-engines, in Table 1. In both cases, the service conditions are severe. But this is especially so for steels where the service life is many decades. The degree of reliability demanded of heat resistant steels is therefore extraordinary, and must represent one of the highest achievements of technology. By contrast, computers, which are frequently identified with advanced technology, seldom last for more than two years and are generally obsolete at the point of installation!

Property	Aeroengine	Power Plant
Temperature	$> 1000\text{ }^{\circ}\text{C}$	540-750 $^{\circ}\text{C}$
Pressure	$\simeq 3\text{ bar}$	160–370 bar
Design life	$10^4\text{ h}$	$2.5 \times 10^5\text{ h}$
$\sigma_{100,000\text{ h}}$	10 MPa	100 MPa
Coating	Yes	No
Forced cooling	Yes	No
Single crystal	Yes	No

Table 1: Service conditions for a component in the hot part of an aeroengine and one in the hottest part of a power plant.

It should not be surprising that the number of variables involved in the design of creep-resistant steels is very large – in fact, we shall show later that there are at least thirty parameters which need to be controlled in any experiment or calculation of creep properties.

The variables can ideally be taken into account using what scientists like to call “physical models”, *i.e.* theories which explain a large class of observations, which contain few arbitrary elements and which make verifiable predictions. The first part of this paper deals with such physical models in the prediction of microstructure.

There is no adequate theory to deal with the second task, which is the estimation of creep rupture strength as a function of the steel composition, microstructure and heat treatment. Difficult problems like this, where the general concepts might be understood but which are not as yet amenable to fundamental treatment, are common in metallurgy. To form a complete design–technology, it is consequently necessary to resort to careful empiricism. The second part of this paper deals with a semi–empirical method implemented to achieve useful results. The combination of physical and empirical models can then be used to attempt the design of alloys.

The final part of the paper deals with the estimation of the self–diffusion coefficient of iron containing solute additions. This is perceived to be an important parameter in creep deformation; it has become prominent in recent work because of the availability of commercial software capable of estimating the diffusivity. It is useful therefore to summarise the basis of such calculations, even though it is too early to comment on their significance in the context of changes in creep properties.

## Microstructure

There is a large variety of heat–resistant steels (Table 2). The ones with the lowest solute concentrations might contain substantial quantities of allotriomorphic ferrite and some pearlite, but the vast majority have bainitic or martensitic microstructures in the normalised condition. After normalising the steels are severely tempered to produce a “stable” microstructure consisting of a variety of alloy carbides in a ferritic matrix. The known precipitates are listed in Fig. 1; they determine the microstructure and are crucial in the development of creep strain. The task is therefore to model the evolution of precipitation and dissolution reactions.

The results of equilibrium calculations which give the phase fractions of the carbides as a function of the overall alloy composition and temperature, are given in Fig. 2 for the common power plant steels. The

## Possible phases

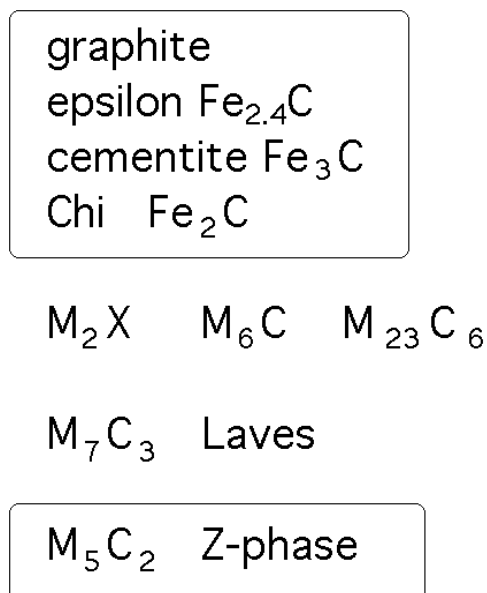


Fig. 1: The variety of precipitates to be found in power plant steels. The iron-rich carbides such as cementite form extremely rapidly, whereas graphite forms incredibly slowly because it is difficult to nucleate.  $\text{M}_5\text{C}_2$  and Z-phase are recent discoveries [2,3].

calculations have been done using the *MTDATA* [1] computer program and *SGTE* database, taking into account the carbide phases and Laves phase listed, together with cementite. The chemical elements considered are carbon, silicon, manganese, chromium, nickel, molybdenum, vanadium, niobium and nitrogen.  $\text{M}_5\text{C}_2$  has recently been identified in 1Cr–0.5Mo steels [2] but along with graphite, has not been included in the analysis.

Equilibrium calculations such as those presented in Fig. 2 are useful in specifying the ultimate microstructure but the results are far from the actual microstructures that exist during service. It is necessary in practice to be able to calculate time–temperature–transformation diagrams for tempering reactions, as a function of steel chemical composition and tempering temperature. In order to do this, a theory capable of handling several simultaneous precipitation reactions has been devel-

Designation	C	Si	Mn	Ni	Mo	Cr	V
1Cr $\frac{1}{2}$ Mo	0.15	0.25	0.50	–	0.6	0.95	
$\frac{1}{4}$ CrMoV	0.15	0.25	0.50	0.05	0.50	0.30	0.25
$\frac{1}{2}$ Cr $\frac{1}{2}$ Mo $\frac{1}{4}$ V	0.12	0.25	0.50	–	0.6	0.45	0.25
1CrMoV	0.25	0.25	0.75	0.70	1.00	1.10	0.35
2 $\frac{1}{4}$ Cr1Mo	0.15	0.25	0.50	0.10	1.00	2.30	0.00
Mod. 2 $\frac{1}{4}$ Cr1Mo	0.1	0.05	0.5	0.16	1.00	2.30	0.25
						Ti=0.03	B=0.0024
3.0Cr1.5Mo	0.1	0.2	1.0	0.1	1.5	3.0	0.1
3.5NiCrMoV	0.24	0.01	0.20	3.50	0.45	1.70	0.10
9Cr1Mo	0.10	0.60	0.40	–	1.00	9.00	–
Mod. 9Cr1Mo	0.1	0.35	0.40	0.05	0.95	8.75	0.22
					Nb=0.08	N=0.05	Al <0.04
9Cr $\frac{1}{2}$ MoWV	0.11	0.04	0.45	0.05	0.50	9.00	0.20
					W=1.84	Nb=0.07	N=0.05
12CrMoV	0.20	0.25	0.50	0.50	1.00	11.25	0.30
12CrMoVW	0.20	0.25	0.50	0.50	1.00	11.25	0.30
							W=0.35
12CrMoVNb	0.15	0.20	0.80	0.75	0.55	11.50	0.28
						Nb 0.30	N 0.06

Table 2: Compositions (wt.% ) of creep-resistant steels.

oped [4], where the different phases influence each other, for example by drawing the same solute from the matrix ferrite.

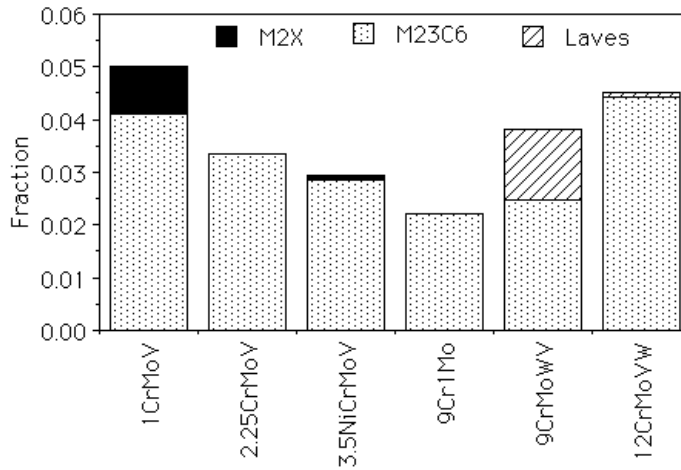


Fig. 2: Equilibrium fractions of carbides in some common power plant steels, as calculated using MTDATA and the SGTE thermodynamic database for 565 °C (838 K). Very small fractions of vanadium and niobium carbonitrides are present in some steels but are not shown. Thus, the modified 9Cr1Mo contains 0.0009 NbN and 0.003 VN, the 9CrMoWV steel contains 0.0008 NbN and 0.0032 VN. The calculations allowed the existence of all the carbides described in Figure 1 with the exception of graphite, epsilon, Chi, Z-phase and  $M_5C_2$ .

### Overall Transformation Kinetics

A model for a single transformation begins with the calculation of the nucleation and growth rates using classical theory, but an estimation of the volume fraction requires impingement between particles to be taken into account. This is generally done using the extended volume concept of Johnson, Mehl, Avrami, and Kolmogorov [5] as illustrated in Fig. 3. Suppose that two particles exist at time  $t$ ; a small interval  $\delta t$  later, new regions marked  $a$ ,  $b$ ,  $c$  &  $d$  are formed assuming that they are able to grow unrestricted in extended space whether or not the region into which they grow is already transformed. However, only those components of  $a$ ,  $b$ ,  $c$  &  $d$  which lie in previously untransformed matrix can contribute to a change in the real volume of the product

phase (identified by the subscript ‘1’) so that :

$$dV_1 = \left(1 - \frac{V_1}{V}\right)dV_1^e \quad (1)$$

where it is assumed that the microstructure develops randomly. The superscript  $e$  refers to extended volume,  $V_1$  is the volume of phase 1 and  $V$  is the total volume. Multiplying the change in extended volume by the probability of finding untransformed regions has the effect of excluding regions such as  $b$ , which clearly cannot contribute to the real change in volume of the product. This equation can easily be integrated to obtain the real volume fraction,

$$\frac{V_1}{V} = 1 - \exp\left\{-\frac{V_1^e}{V}\right\} \quad (2)$$

Nucleation and growth rates can readily be substituted into  $V_1^e$ , leading to the familiar Avrami equation.

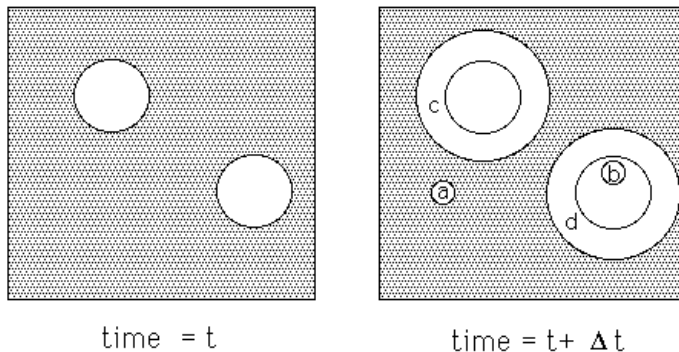


Fig. 3: The concept of extended volume. Two precipitate particles have nucleated and grown to a finite size in the time  $t$ . New regions  $c$  and  $d$  are formed as the original particles grow, but  $a$  &  $b$  are new particles, of which  $b$  has formed in a region which is already transformed.

In practice, there are many cases where several transformations occur together. The different reactions interfere with each other in a

way which is seminal to the development of power plant microstructures. The principles involved are first illustrated with an example in which  $\beta$  and  $\theta$  precipitate at the same time from the parent phase which is designated  $\alpha$ . For the sake of discussion it is assumed that the nucleation and growth rates do not change with time and that the particles grow isotropically.

The increase in the extended volume due to particles nucleated in a time interval  $t = \tau$  to  $t = \tau + d\tau$  is, therefore, given by

$$dV_{\beta}^e = \frac{4}{3}\pi G_{\beta}^3(t - \tau)^3 I_{\beta}(V) d\tau \quad (3)$$

$$dV_{\theta}^e = \frac{4}{3}\pi G_{\theta}^3(t - \tau)^3 I_{\theta}(V) d\tau \quad (4)$$

where  $G_{\beta}$ ,  $G_{\theta}$ ,  $I_{\beta}$  and  $I_{\theta}$  are the growth and nucleation rates of  $\beta$  and  $\theta$  respectively, all of which are assumed here to be independent of time.  $V$  is the total volume of the system. For each phase, the increase in extended volume will consist of three separate parts. Thus, for  $\beta$ :

- (i)  $\beta$  which has formed in untransformed  $\alpha$ .
- (ii)  $\beta$  which has formed in regions which are already  $\beta$ .
- (iii)  $\beta$  which has formed in regions which are already  $\theta$ .

Only  $\beta$  formed in untransformed  $\alpha$  will contribute to the real volume of  $\beta$ . On average a fraction  $\left(1 - \frac{V_{\beta} + V_{\theta}}{V}\right)$  of the extended volume will be in previously untransformed material. It follows that the increase in real volume of  $\beta$  is given by

$$dV_{\beta} = \left(1 - \frac{V_{\beta} + V_{\theta}}{V}\right) dV_{\beta}^e \quad (5)$$

and similarly for  $\theta$ ,

$$dV_{\theta} = \left(1 - \frac{V_{\beta} + V_{\theta}}{V}\right) dV_{\theta}^e \quad (6)$$

$V_{\beta}$  is expected to be some complicated function of  $V_{\theta}$  so it is not generally possible to integrate these expressions analytically to find the relationship between the real and extended volumes. Numerical integration is

straightforward and offers the opportunity to change the boundary conditions for nucleation and growth as transformation proceeds, to account for the change in the matrix composition during the course of reaction. The method can in principle be applied to any number of simultaneous reactions.

**Complex reactions** The multiple reactions found in power plant steels have important complications which can all be dealt with in the scheme of simultaneous transformations as presented above. The phases interfere with each other not only by reducing the volume available for transformation, but also by removing solute from the matrix and thereby changing its composition. This change in matrix composition affects the growth and nucleation rates of the phases. The main features of the application of the theory to power plant steels are summarised below; a full description is given in references [4].

- The model allows for the simultaneous precipitation of  $M_2X$ ,  $M_{23}C_6$ ,  $M_7C_3$ ,  $M_6C$  and Laves phase.  $M_3C$  is assumed to nucleate instantaneously with the paraequilibrium composition [6]. Subsequent enrichment of  $M_3C$  as it approaches its equilibrium composition is accounted for.
- All the phases, except  $M_3C$ , form close to their equilibrium composition. The driving forces and compositions of the precipitating phases are calculated using MTDATA [1].
- The interaction between the precipitating phases is accounted for by considering the change in the average solute level in the matrix as each phase forms.
- The model does not require prior knowledge of the precipitation sequence.
- Dissolution of non-equilibrium phases is incorporated as a natural event.
- A single set of fitting parameters for the nucleation equations (site densities and surface energies) has been found which is applicable to a wide range of power plant steels.

The compositions of three power plant alloys used here for illustration purposes, are shown in Table 3. These three alloys, whilst of quite different chemical compositions, show similar precipitation *sequences* [4,7,8] but with vastly different rates. For example, at 600 °C the time taken before  $M_{23}C_6$  is observed is 1 h in the 10CrMoV steel [4], 10 h in the 3Cr1.5Mo alloy [7] and in excess of 1000 h in the  $2\frac{1}{4}$ Cr1Mo steel

[8]. These differences have never before been explained prior to the simultaneous transformations model [4].

	C	N	Mn	Cr	Mo	Ni	V	Nb
$2\frac{1}{4}\text{Cr1Mo}$	0.15	–	0.50	2.12	0.9	0.17	–	–
$3\text{Cr1.5Mo}$	0.1	–	1.0	3.0	1.5	0.1	0.1	–
$10\text{CrMoV}$	0.11	0.056	0.50	10.22	1.42	0.55	0.20	0.50

Table 3: Concentration (in weight%) of the major alloying elements in the steels used to demonstrate the model.

## MICROSTRUCTURE CALCULATIONS

A plot showing the predicted variation of volume fraction of each precipitate as a function of time at 600 °C is shown in Fig. 4. Consistent with experiments, the precipitation kinetics of  $M_{23}C_6$  are predicted to be much slower in the  $2\frac{1}{4}\text{Cr1Mo}$  steel compared to the  $10\text{CrMoV}$  and  $3\text{Cr1.5Mo}$  alloys. One contributing factor is that in the  $2\frac{1}{4}\text{Cr1Mo}$  steel a relatively large volume fraction of  $M_2X$  and  $M_7C_3$  form prior to  $M_{23}C_6$ . These deplete the matrix and therefore suppress  $M_{23}C_6$  precipitation. The volume fraction of  $M_2X$  which forms in the  $10\text{CrMoV}$  steel is relatively small, and there remains a considerable excess of solute in the matrix, allowing  $M_{23}C_6$  to precipitate rapidly. Similarly, in the  $3\text{Cr1.5Mo}$  steel the volume fractions of  $M_2X$  and  $M_7C_3$  are insufficient to suppress  $M_{23}C_6$  precipitation to the same extent as in the  $2\frac{1}{4}\text{Cr1Mo}$  steel.

$M_{23}C_6$  is frequently observed in the form of coarse particles which are less effective in hindering creep deformation. Delaying its precipitation would have the effect of stabilising the finer dispersions of  $M_2X$  and  $MX$  to longer times with a possible enhancement of creep strength.

Calculations like these can be used to design microstructures exploiting knowledge built up over decades concerning what is good and bad for creep strength. It is often argued that Laves phase formation is bad for creep resistance – it leads to a reduction in the concentration of solid solution strengthening elements; since the Laves precipitates are few and coarse, they do not themselves contribute significantly to

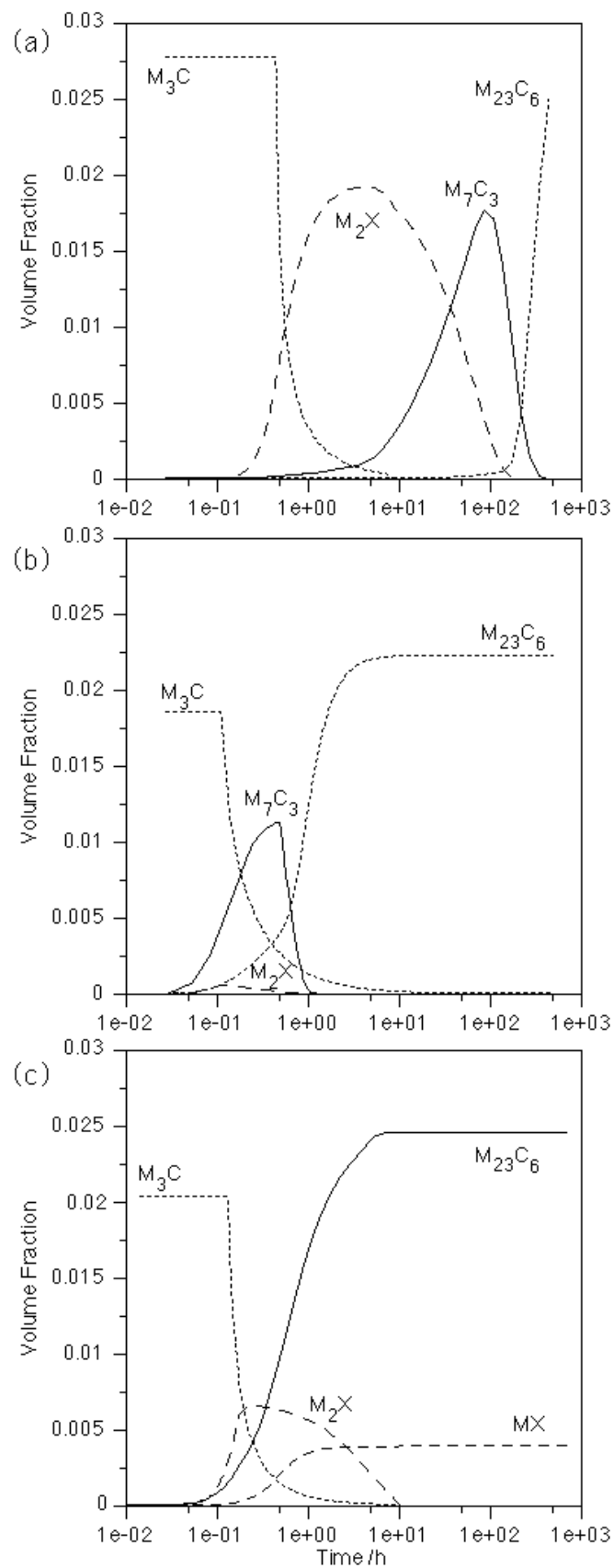


Fig. 4: The predicted evolution of precipitate volume fractions at 600 °C for three power plant materials (a) 2 1/4Cr1Mo (b) 3Cr1.5Mo and (c) 10CrMoV.

strength. The model presented here can be used to design against Laves phase formation.

We note for the moment, that this is as far as microstructure modelling has progressed. The models are not yet capable of giving size distributions and even if that were to be possible, there are no physical models of creep deformation which have sufficient precision to make use of this information. We shall not be discouraged by this since good empirical methods are available. The work described below originates from research by Brun *et al.* [9] and Cole and Bhadeshia [10].

### **Creep Rupture - the variables**

The basic principles of alloy design for creep resistance are well-established and well-founded on experience. The steels must have a stable microstructure which contains fine alloy carbides to resist the motion of dislocations; however, changes are inevitable over the long service time so that there must be sufficient solid solution strengthening to ensure long term creep resistance. There may be other requirements such as weldability, corrosion and oxidation resistance. It is nevertheless difficult to express the design process quantitatively given the large number of interacting variables.

These variables are described later in the context of calculations in Table 4. For the moment we note that the entire information about microstructure and properties is in principle locked up in this set of parameters since chemical composition and heat treatment are comprehensively included. There may, of course, be many other independent variables that might be considered important in creep analysis, but these are for the moment neglected for two reasons. Firstly, an empirical analysis requires experimental data; an over ambitious list would simply reduce the dataset since publications frequently do not report all of the necessary parameters. Secondly, the effect of any missing variables would simply be reflected in the uncertainties of prediction. If the predictions are noisy then they can be improved with carefully designed experiments at a future date. Bearing this in mind, the results to be presented are based on some 2000 sets of experiments obtained from the published literature. We now proceed to describe briefly the methodology.

### **Neural Network Method**

Most people are familiar with regression analysis where data are best-fitted to a specified relationship which is usually linear. The result

is an equation in which each of the inputs  $x_j$  is multiplied by a weight  $w_j$ ; the sum of all such products and a constant  $\theta$  then gives an estimate of the output  $y = \sum_j w_j x_j + \theta$ . It is well understood that there are dangers in using such relationships beyond the range of fitted data.

A more general method of regression is neural network analysis. As before, the input data  $x_j$  are multiplied by weights, but the sum of all these products forms the argument of a hyperbolic tangent. The output  $y$  is therefore a non-linear function of  $x_j$ , the function usually chosen being the hyperbolic tangent because of its flexibility. The exact shape of the hyperbolic tangent can be varied by altering the weights (Fig. 5a). Further degrees of non-linearity can be introduced by combining several of these hyperbolic tangents (Fig. 5b), so that the neural network method is able to capture almost arbitrarily non-linear relationships. For example, it is well known that the effect of chromium on the microstructure of steels is quite different at large concentrations than in dilute alloys. Ordinary regression analysis cannot cope with such changes in the form of relationships.

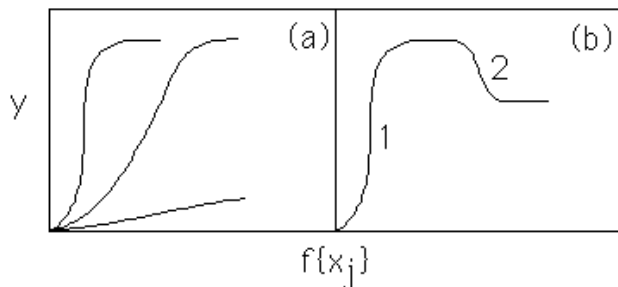


Fig. 5: (a) Three different hyperbolic tangent functions; the “strength” of each depends on the weights. (b) A combination of two hyperbolic tangents to produce a more complex model.

A potential difficulty with the use of powerful regression methods is the possibility of overfitting data (Fig. 6). For example, one can produce a neural network model for a completely random set of data. To avoid this difficulty, the experimental data can be divided into two sets, a *training* dataset and a *test* dataset. The model is produced using only the training data. The test data are then used to check that the model behaves itself when presented with previously unseen data.

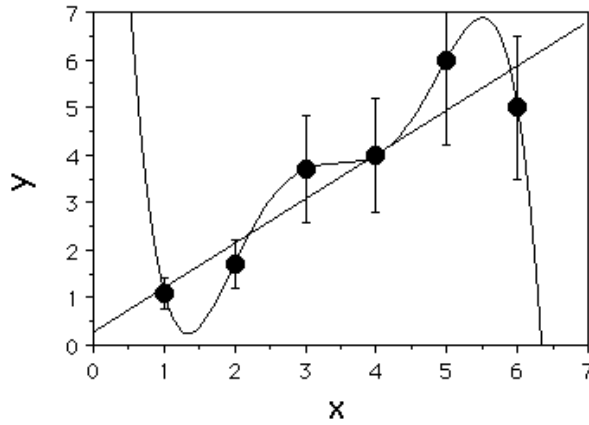


Fig. 6: A complicated model may overfit the data. In this case, a linear relationship is all that is justified by the noise in the data.

Neural network models in many ways mimic human experience and are capable of learning or being trained to recognise the correct science rather than nonsensical trends. Unlike human experience, these models can be transferred readily between generations and steadily developed to make design tools of lasting value. These models also impose a discipline on the digital storage of valuable experimental data, which may otherwise be lost with the passage of time.

The technique is extremely powerful and useful. Its application to creep rupture strength analysis is presented below. The details can be found elsewhere [11] but it is important to note that the generalisation of the model on unseen data has been tested extensively against large quantities of information.

### Calculations of Creep Rupture Strength

Fig. 7 shows the variation in the creep rupture strength ( $10^5$  h) of a modern “10CrMoW” creep resistant steel (Table 4) as a function of the temperature, carbon, chromium and molybdenum concentrations. The error bounds represent the uncertainty in fitting the non-linear function to the training data, as 65% confidence limits. There is an additional error associated with each calculation, which is the noise in the experimental data, which is perceived to be of the order of  $\pm 2\%$ . The engineering design of power plant is based on the ability to support a stress of 100 MPa for  $10^5$  h at the service temperature. The

apparent insensitivity of the creep rupture strength to the molybdenum or chromium concentrations for  $10^5$  h is not surprising given that the carbides will all be extremely coarse at that stage of life.

Similar data for the classical  $2\frac{1}{4}\text{Cr1Mo}$  steel are illustrated in Fig. 8. The fitting uncertainties are smaller in this case because of the larger quantity of available data since this alloy has been available and studied for a much longer time.

Calculations like these can now be routinely carried out. Furthermore, the models can be improved both as more data become available and as creep deformation becomes better understood. The model can be used in a variety of ways. The combined application of the physical models presented earlier, and the neural network model has led to predictions of novel alloys which ought to have much better creep resistance than any comparable commercial alloy [9]. There are long-term experiments in progress to test these designer-alloys. Another way is to apply the models to welding alloys, for which there are much fewer data when compared with wrought steels.

## Conclusions

It is now possible to attempt a quantitative design of heat resistant steels and welding alloys. This is true both with respect to the kinetics of microstructural evolution and in the estimation of creep rupture strength. The combined models provide for the first time an ability to predict new alloys. It would now be interesting for industry to set some challenges, which would stimulate theoretical predictions and finally experimental verification. The whole process from the conception of an alloy to its verification should take much less time than has previously been the case.

In the longer term it is necessary for the microstructure models to predict particle size and spatial distributions, and the effect of stress and strain on transformation kinetics. Such information can then be used in a more sophisticated mechanical model, perhaps based on dislocation and recovery theory.

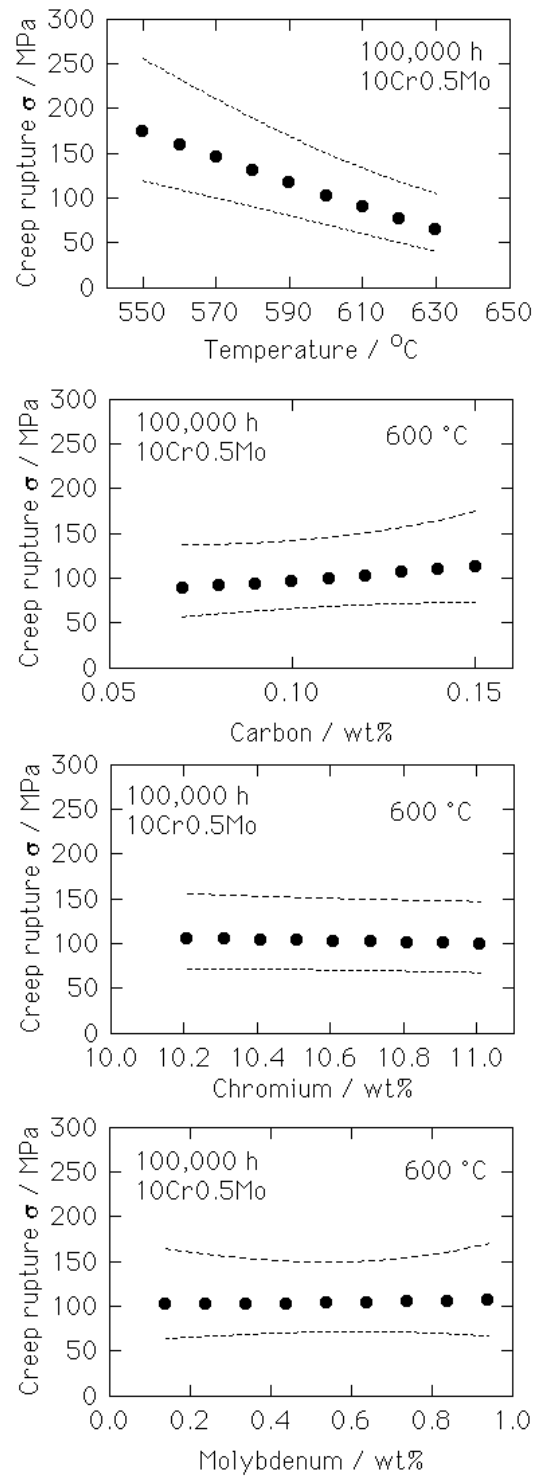


Fig. 7: Creep rupture stress at 600 °C and 100,000 h for 10Cr–0.5Mo type steel

STEEL	$2\frac{1}{4}\text{CrMo}$	10CrMoW
Normalising temperature / K	1203	1338
Duration / h	6	2
Cooling rate	water quenched	air cooled
Tempering temperature / K	908	1043
Duration / h	6	4
Cooling rate	air cooled	air cooled
Annealing temperature / K	873	1013
Duration / h	2	4
Cooling rate	air cooled	air cooled
C wt%	0.15	0.12
Si	0.21	0.05
Mn	0.53	0.64
P	0.012	0.016
S	0.012	0.001
Cr	2.4	10.61
Mo	1.01	0.44
W	0.01	1.87
Ni	0.14	0.32
Cu	0.16	0.86
V	0.01	0.21
Nb	0.005	0.01
N	0.0108	0.064
Al	0.018	0.022
B	0.0003	0.0022
Co	0.05	0.015
Ta	0.0003	0.0003
O	0.01	0.01

Table 4: The standard set of input parameters for two alloys used to examine trends predicted by the neural network. The chemical compositions are all in wt.%

## References

1. MTDATA: *Metallurgical Thermochemistry Group*, National Physical Laboratory, Teddington, London (1998)
2. S. D. Mann, D. G. McCulloch and B. C. Muddle: *Metallurgical and Materials Transactions A* 26A, 509–520(1995)
3. A. Strang and V. Vodarek: *Materials Science and Technology*, 12, 552–556.(1996)
4. J. D. Robson and H. K. D. H. Bhadeshia: *Mat. Sci. Tech.* 13, 631–644(1997)
5. J. W. Christian: *Theory of Transformations in Metals and Alloys*, Pergamon Press, Oxford, 2nd edition, part I (1975)
6. H. K. D. H. Bhadeshia: *Materials Science and Technology* 5, 131–137.(1989)
7. N. Fujita and H. K. D. H. Bhadeshia: *Advanced Heat Resistant Steels for Power Generation*, San Sebastian, published by the Institute of Materials, London, in press.(1998)
8. R. G. Baker and J. Nutting: *Journal of the Iron and Steel Institute* 192, 257–268(1959)
9. F. Brun, T. Yoshida, J. D. Robson, V. Narayan and H. K. D. H. Bhadeshia: *Materials Science and Technology* submitted(1998)
10. D. Cole and H. K. D. H. Bhadeshia: *Unpublished research*, University of Cambridge (1998)
11. D. J. C. MacKay: *Neural Computation* 4, 415-472(1992)

